Quest: Journal of Geometry, Mathematical and Quantum Physics
e-ISSN: 3064-7282 Vol.2 Issue 6|2025

# Calculation the Nuclear Radiation Absorption Parameters in Pb Alloys

**Sufyan Saadi Hussein, Sabah Mahmoud Aman Allah**
Department of Physics-College of Education for Pure Sciences-University of Kirkuk-Kirkuk-Iraq

**Abstract:** In this research, various binary alloys were prepared and studied, consisting of lead as the matrix material, with different weight percentages of bismuth and tin added as enhancing elements. The study focused on evaluating the physical properties of these alloys, specifically their ability to attenuate gamma rays. For this purpose, the mass attenuation coefficient ($\mu_m$) of the prepared alloys was calculated using the Nist-XCom database, over a wide energy range from 0.05953 to 800(MeV). Based on the calculated mass attenuation coefficient values, a set of other important attenuation parameters were derived, including the linear attenuation coefficient ($\mu$), molecular cross section ($\sigma_m$), electron cross section ($\sigma_{ele}$), effective atomic number ($Z_{eff}$), electron density ($N_{ele}$), mean free path ($\lambda$), half-layer thickness (HVL), and tenth-layer thickness (TVL). In addition, the K-edge absorption edges of the elements in the studied alloys were determined.

**Keywords:** Gamma ray, Half, tenth, quarter, layer, Linear attenuation coefficient, Mass attenuation coefficient, Molecular cross-section, NIST-XCOM.

## 1. Introduction

To ensure the safe use of ionizing radiation, researchers are increasingly focusing on developing effective shielding materials. The effectiveness of these materials is measured by their ability to reduce radiation transmittance. Therefore, extensive studies are being conducted on the radiation attenuation properties of various materials to identify the most efficient ones. The main physical properties evaluated include the mass and linear attenuation coefficient, molecular and electron interaction cross-sectional area, effective atomic number, electron density, mean free path, as well as half- and decimal layer thicknesses [1].

In 2008, Saxby-Brown et al. conducted a study to investigating the correlation between linear attenuation coefficients and Hounsfield units (HUs). Six different materials were examined, representing the range of values found in clinical practice [2].

A study conducted by Ali H. Taqi et al. in 2021 on ternary alloys of (lead, tin, copper) at varying weight ratios determined their protective properties. These properties included molecular and electronic cross sections ($\sigma_m$ and $\sigma_{ele}$), which were consistent with known experimental values [3].

Using the 662 keV gamma ray backscatter technique, Sharma et al. in 2016 were able to calculate the atomic numbers of a group of binary alloys. The study included lead-tin, lead-zinc, and tin-zinc alloys with varying weight ratios [4].

According to a 2016 study, Kaur et al. calculated the average free path values for several types of heavy metal oxide glasses [5].

In a study published in 2009, Han and Demir were able to determine the values of two critical parameters in metal alloys, namely the effective atomic number and electron density, in alloys consisting of titanium (Ti), copper (Cu), and nickel (Ni) [6].

Tejbir Singh and his research team in 2018 prepared binary lead-copper alloys of different weight ratios, analyzed their physical properties and gamma ray attenuation parameters, especially half-thickness and ten-thickness layers [7].

## 2. Materials and Methods

In the current study, calculations were performed for some binary metal alloys with varying proportions of their components to form mixtures to select the best of these materials for the manufacture of gamma ray shields. The atomic numbers of the selected elements in the alloy composition are: Pb=82 , Sn=50 and Bi=83.

The density of each alloy was calculated from the law for finding the density of mixtures and according to the following equation :

$$P_w = \sum \rho_i * w_i = \rho_1 w_1 + \rho_2 w_2 + \rho_3 w_3 + \ldots\ldots \quad (1)$$

The molar mass of each alloy can be calculated from the law for finding the molar mass of mixtures and according to the following equation :

$$M_w = \sum M_i * w_i = M_1 w_1 + M_2 w_2 + M_3 w_3 + \ldots\ldots\ldots \quad (2)$$

**Table 1: Molecular weights and densities of the alloys under study.**

| Binary alloys | Samples | % | $\rho\ (\frac{g}{cm^3})$ | M (g/mole) |
|---|---|---|---|---|
| Pb-Sn | S1 | 60Pb40Sn | 9.728 | 171.804 |
| | S2 | 70Pb30Sn | 10.131 | 180.653 |
| | S3 | 80Pb20Sn | 10.534 | 189.502 |
| Pb-Bi | S4 | 60Pb40Bi | 10.716 | 207.912 |
| | S5 | 70Pb30Bi | 10.872 | 207.734 |
| | S6 | 80Pb20Bi | 11.028 | 207.556 |

The results showed a direct relationship between the lead concentration in the alloys and both the density and theoretical molecular weight, with both properties gradually increasing with increasing lead content. This behavior is explained by the physical nature of lead, which has a higher density and atomic mass than the other alloy components, which positively impacts the overall values of these parameters as its content increases.

The mass attenuation coefficient ($\mu_m$) is a measure used to determine the probability of an incident photon interacting with a material, and is measured in $cm^2/g$. This coefficient is a non-constant quantity, as it varies depending on the energy of the incident photon and the atomic number of the elements or the effective atomic number in the case of compounds and mixtures, while it is not affected by the physical state of the material. It is calculated using the NIST-XCom database for the elements $_{82}Pb$, $_{83}Bi$, and $_{50}Sn$, over an energy range of 0.05953 to 800 MeV [10].

Molecular cross-sectional area indicates the extent to which the molecules of a substance are able to interact with the incoming particle, and is used as an indicator of the likelihood of this interaction occurring [11].

$$\sigma_m = \mu_m \frac{M}{N_A} \quad (3)$$

The electron cross-sectional area indicates the extent to which an interaction between an incident particle and the orbital electrons of an atom of the target material is likely to occur [11].

$$\sigma_{ele} = \frac{1}{N_A}\sum_i f_i \frac{A_i}{Z_i} (\mu_m)_i \quad (4)$$

In mixtures the sum of the number of atoms is always one $\sum_i n_i = 1$, so the values of $\sigma_m$ and $\sigma_a$ are equal

$\sigma_m = \sigma_a$[12].

Linear attenuation coefficient (μ) The probability of a photon loss of a gamma ray beam is a result of various reactions as it passes through the material, under ideal geometric conditions for the measurement process, as it is assumed that any reaction can contribute to removing the photon from the radiation beam[11].

$$\mu = \mu_m x \rho \quad (5)$$

The atomic number ($Z_{eff}$) represents a value close to the true atomic number of elements, and is used as a main indicator to assess the ability of materials to protect against radiation. It is also an important tool for analyzing gamma rays when it penetrates into composite materials or mixtures[12].

$$Z_{eff} = \frac{\sigma_a}{\sigma_e} \quad (6)$$

The electron density is an important factor in radiation protection, as it represents the average number of electrons per unit mass in the reaction subject[12].

$$N_{ele} = \frac{\mu_m}{\sigma_{ele}} \quad (7)$$

The mean free path (MFP) expresses the expected distance a photon travels within a material before undergoing an interaction such as scattering or absorption, and is usually measured in centimeters [13].

$$\lambda = \frac{1}{\mu} \quad (8)$$

Half-value layer (HVL) [14]

$$HVL = \ln(2)/\mu \quad (9)$$

Tenth-value layer (TVL)

$$TVL = \ln(10)/\mu \quad (10)$$

## 3. Calculation

Mass attenuation coefficient values were calculated from the Nist XCom database for $_{82}$Pb, $_{83}$Bi, and $_{50}$Sn in the energy range of (0.05953-800 ) MeV.

**Table 2: Mass attenuation coefficient values were calculated using the Nist XCom database .**

| E(MeV) | μ (cm²/g) | | | | | |
|---|---|---|---|---|---|---|
| | S1 | S2 | S3 | S4 | S5 | S6 |
| 0.05953 | 5.755 | 5.597 | 5.439 | 5.209 | 5.187 | 5.166 |
| 0.08099 | 2.58 | 2.522 | 2.463 | 2.386 | 2.376 | 2.366 |
| 0.12178 | 2.433 | 2.67 | 2.907 | 3.428 | 3.416 | 3.405 |
| 0.24469 | 0.4655 | 0.5056 | 0.5457 | 0.6346 | 0.6324 | 0.6303 |
| 0.35601 | 0.225 | 0.2406 | 0.2562 | 0.2909 | 0.29 | 0.2891 |
| 0.364 | 0.2166 | 0.2314 | 0.2461 | 0.279 | 0.2781 | 0.2773 |
| 0.66166 | 0.09636 | 0.09982 | 0.1033 | 0.1112 | 0.1109 | 0.1107 |
| 0.7789 | 0.08189 | 0.08424 | 0.08659 | 0.092 | 0.09182 | 0.09165 |
| 0.96413 | 0.06782 | 0.06923 | 0.07065 | 0.07396 | 0.07384 | 0.07372 |

| | | | | | | |
|---|---|---|---|---|---|---|
| 1.17323 | 0.05815 | 0.05905 | 0.05995 | 0.06208 | 0.062 | 0.06191 |
| 1.25 | 0.05563 | 0.05641 | 0.05719 | 0.05907 | 0.05899 | 0.05891 |
| 1.3325 | 0.05338 | 0.05407 | 0.05476 | 0.05643 | 0.05636 | 0.05629 |
| 1.40801 | 0.05165 | 0.05229 | 0.05292 | 0.05445 | 0.05439 | 0.05432 |
| 2.75 | 0.0407 | 0.04123 | 0.04176 | 0.04299 | 0.04295 | 0.0429 |
| 7.12 | 0.0419 | 0.04279 | 0.04368 | 0.04566 | 0.04561 | 0.04556 |
| 10 | 0.04541 | 0.04649 | 0.04757 | 0.04993 | 0.04988 | 0.04983 |
| 20 | 0.05588 | 0.05742 | 0.05897 | 0.06234 | 0.06227 | 0.0622 |
| 30 | 0.06294 | 0.06476 | 0.06658 | 0.07055 | 0.07047 | 0.07039 |
| 40 | 0.06804 | 0.07006 | 0.07207 | 0.07646 | 0.07637 | 0.07628 |
| 50 | 0.07192 | 0.07408 | 0.07624 | 0.08094 | 0.08085 | 0.08075 |
| 60 | 0.07502 | 0.07728 | 0.07955 | 0.08448 | 0.08438 | 0.08428 |
| 70 | 0.07753 | 0.07989 | 0.08224 | 0.08737 | 0.08726 | 0.08716 |
| 80 | 0.07963 | 0.08206 | 0.08449 | 0.08977 | 0.08966 | 0.08955 |
| 90 | 0.08142 | 0.08391 | 0.08639 | 0.0918 | 0.09169 | 0.09158 |
| 100 | 0.08296 | 0.0855 | 0.08803 | 0.09354 | 0.09343 | 0.09332 |
| 200 | 0.09148 | 0.09428 | 0.09709 | 0.1032 | 0.1031 | 0.1029 |
| 300 | 0.09525 | 0.09816 | 0.1011 | 0.1074 | 0.1073 | 0.1072 |
| 400 | 0.09742 | 0.1004 | 0.1034 | 0.1099 | 0.1097 | 0.1096 |
| 500 | 0.09885 | 0.1019 | 0.1049 | 0.1115 | 0.1113 | 0.1112 |
| 600 | 0.09989 | 0.1029 | 0.106 | 0.1126 | 0.1125 | 0.1123 |
| 700 | 0.1007 | 0.1037 | 0.1068 | 0.1135 | 0.1133 | 0.1132 |
| 800 | 0.1013 | 0.1044 | 0.1074 | 0.1142 | 0.114 | 0.1139 |

Fig 1 shows the absorption edges ( K-edge), known as the Compton edges, for the studied samples. These edges represent the sharp dip in the gamma-ray absorption spectrum resulting from the interaction of photons with the energy levels of electrons within atoms. This occurs when the energy of the incident photon approaches the binding energy of the electrons in the atomic shell. This sudden change in attenuation is attributed to photoelectric absorption, which requires the energy of the photons to be slightly higher than the binding energy of the electrons [15].

The absorption edges of lead metal are clearly visible, with the M edge located between 0.002484 and 0.003851, the L edge between 0.01304 and 0.01586, and the K edge located at 0.088. In bismuth, the M edge lies between 0.00258 and 0.003999, the L edge between 0.01342 and 0.01639, and the K edge is recorded at 0.09053. Tin, on the other hand, has an L edge between 0.003929 and 0.004465, and a K edge at 0.2920.

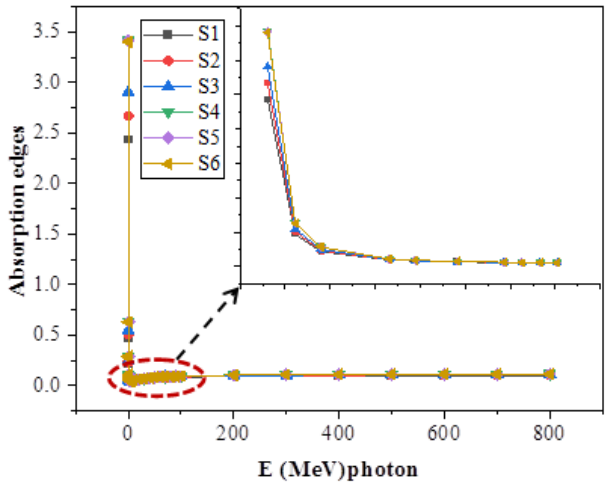


**Fig 1. Absorption edges of the samples under study.**

Fig 2 illustrates the behavior of the mass attenuation coefficient of the studied samples depending on the incident photon energy. The graph shows an inverse relationship between the mass attenuation coefficient and photon energy; the higher the incident photon energy, the lower the attenuation, and vice versa.

The results also showed that sample S4, composed of (60Pb40Bi), recorded the highest mass attenuation coefficient value. This is attributed to its high content of lead and bismuth, known for their high density, large atomic numbers, and large interaction cross-sectional areas, which enhance the material's ability to absorb gamma rays. In contrast, sample S1, composed of (60Pb40Sn), recorded the lowest mass attenuation coefficient value due to its lower lead content compared to the other samples and its higher tin content, which has a lower atomic number and lower density than lead and bismuth.

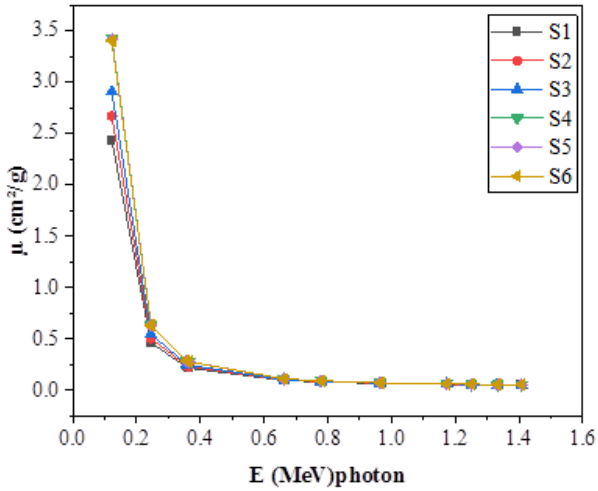


**Fig 2: Mass attenuation coefficient of the samples under study as a function of incident photon energies.**

**Table 3: Evaluate the molecular cross section with incident photon energies.**

| E(MeV) | $\sigma_m$ (Barn/molecule) | | | | | |
|---|---|---|---|---|---|---|
| | S1 | S2 | S3 | S4 | S5 | S6 |
| 0.05953 | 1641.594 | 1678.756 | 1711.276 | 1798.131 | 1789.004 | 1780.234 |
| 0.08099 | 735.9361 | 756.4451 | 774.9351 | 823.6401 | 819.4858 | 815.3373 |
| 0.12178 | 694.0049 | 800.836 | 914.6311 | 1183.335 | 1178.183 | 1173.383 |
| 0.24469 | 132.7823 | 151.6489 | 171.6939 | 219.062 | 218.1157 | 217.205 |
| 0.35601 | 64.18047 | 72.16522 | 80.60836 | 100.4178 | 100.0214 | 99.62554 |
| 0.364 | 61.7844 | 69.40578 | 77.43059 | 96.30997 | 95.91708 | 95.55919 |
| 0.66166 | 27.48636 | 29.93987 | 32.50134 | 38.38591 | 38.24957 | 38.14786 |
| 0.7789 | 23.35884 | 25.26683 | 27.24386 | 31.75813 | 31.66885 | 31.58312 |
| 0.96413 | 19.34542 | 20.76475 | 22.22865 | 25.53077 | 25.46752 | 25.40434 |
| 1.17323 | 16.58709 | 17.71137 | 18.8621 | 21.42983 | 21.38389 | 21.33455 |
| 1.25 | 15.86827 | 16.91953 | 17.99372 | 20.39079 | 20.34573 | 20.30073 |
| 1.3325 | 15.22646 | 16.21768 | 17.22917 | 19.47947 | 19.43864 | 19.39786 |
| 1.40801 | 14.73298 | 15.68379 | 16.65025 | 18.79598 | 18.75919 | 18.71899 |
| 2.75 | 11.60953 | 12.36647 | 13.13897 | 14.84002 | 14.81352 | 14.78359 |
| 7.12 | 11.95183 | 12.83437 | 13.74306 | 15.7617 | 15.73095 | 15.70024 |
| 10 | 12.95305 | 13.94414 | 14.96698 | 17.23569 | 17.20368 | 17.17171 |
| 20 | 15.93958 | 17.22247 | 18.55377 | 21.51958 | 21.47701 | 21.43448 |
| 30 | 17.95342 | 19.42402 | 20.9481 | 24.35365 | 24.3052 | 24.2568 |
| 40 | 19.40818 | 21.0137 | 22.67543 | 26.39376 | 26.34012 | 26.28653 |

| | | | | | | |
|---|---|---|---|---|---|---|
| 50 | 20.51493 | 22.21945 | 23.98744 | 27.94025 | 27.88528 | 27.82692 |
| 60 | 21.3992 | 23.17925 | 25.02886 | 29.16224 | 29.10278 | 29.04338 |
| 70 | 22.11517 | 23.96209 | 25.87522 | 30.15986 | 30.0961 | 30.03584 |
| 80 | 22.71418 | 24.61296 | 26.58314 | 30.98834 | 30.92386 | 30.85945 |
| 90 | 23.22477 | 25.16785 | 27.18094 | 31.68909 | 31.62401 | 31.559 |
| 100 | 23.66405 | 25.64475 | 27.69693 | 32.28973 | 32.22414 | 32.15861 |
| 200 | 26.09435 | 28.27821 | 30.54748 | 35.62433 | 35.55934 | 35.45994 |
| 300 | 27.16973 | 29.44197 | 31.80915 | 37.07416 | 37.00792 | 36.94174 |
| 400 | 27.78872 | 30.11383 | 32.5328 | 37.93715 | 37.83568 | 37.7688 |
| 500 | 28.19662 | 30.56374 | 33.00475 | 38.48947 | 38.38753 | 38.32017 |
| 600 | 28.49328 | 30.86368 | 33.35084 | 38.86918 | 38.80141 | 38.69923 |
| 700 | 28.72433 | 31.10363 | 33.60255 | 39.17986 | 39.07733 | 39.00938 |
| 800 | 28.89548 | 31.31359 | 33.79132 | 39.4215 | 39.31876 | 39.2506 |

Fig 3 shows the changes in molecular cross-sectional area of the studied samples depending on the incident photon energies. The results indicate a direct relationship between the molecular cross-sectional area and the molecular weight fraction of the samples; the higher the molecular weight fraction, the higher the molecular cross-sectional area, and vice versa.

The results showed that sample S4, composed of (60Pb40Bi), had the highest molecular cross-sectional area. This is attributed to the fact that this sample has the highest molecular weight fraction value (207.912) among all the samples. In contrast, sample S1, composed of (60Pb40Sn), recorded the lowest molecular cross-sectional area due to its lower molecular weight fraction (171.804) compared to the other samples.

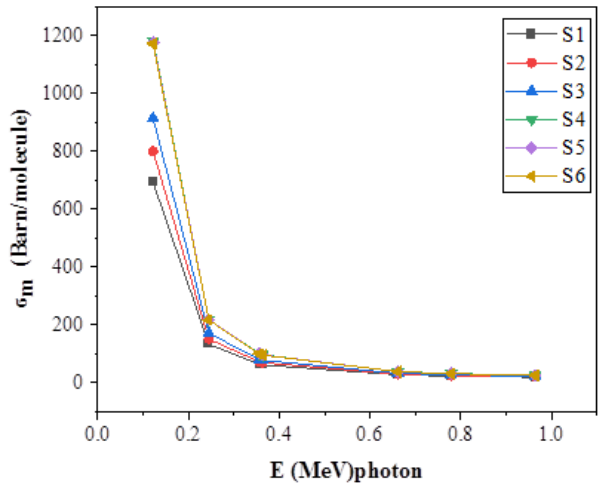


**Fig 3: Molecular cross-sectional area of the studied samples as a function of incident photon energies.**

**Table 4: Evaluate the electron cross section with incident photon energies**

| E(MeV) | $\sigma_{ele}$ (Barn/electron) | | | | | |
|---|---|---|---|---|---|---|
| | S1 | S2 | S3 | S4 | S5 | S6 |
| 0.05953 | 23.5606 | 23.05559 | 22.54258 | 21.82221 | 21.73779 | 21.65749 |
| 0.08099 | 10.56235 | 10.38882 | 10.20819 | 9.995736 | 9.95739 | 9.919015 |
| 0.12178 | 9.960546 | 10.99847 | 12.0484 | 14.36102 | 14.31584 | 14.27483 |
| 0.24469 | 1.905727 | 2.082706 | 2.261718 | 2.658547 | 2.650275 | 2.642415 |
| 0.35601 | 0.921136 | 0.991098 | 1.061851 | 1.218675 | 1.215338 | 1.211998 |
| 0.364 | 0.886747 | 0.953201 | 1.01999 | 1.168822 | 1.165467 | 1.162529 |
| 0.66166 | 0.394492 | 0.411186 | 0.428139 | 0.465853 | 0.464762 | 0.464089 |

| | | | | | | |
|---|---|---|---|---|---|---|
| 0.7789 | 0.335252 | 0.347008 | 0.358882 | 0.385418 | 0.384801 | 0.384226 |
| 0.96413 | 0.277651 | 0.285178 | 0.292817 | 0.309843 | 0.30945 | 0.309057 |
| 1.17323 | 0.238062 | 0.243243 | 0.24847 | 0.260073 | 0.259831 | 0.259546 |
| 1.25 | 0.227746 | 0.232368 | 0.237031 | 0.247464 | 0.247217 | 0.246969 |
| 1.3325 | 0.218534 | 0.222729 | 0.226959 | 0.236404 | 0.236195 | 0.235985 |
| 1.40801 | 0.211452 | 0.215397 | 0.219333 | 0.228109 | 0.227939 | 0.227726 |
| 2.75 | 0.166623 | 0.169838 | 0.173079 | 0.180099 | 0.179996 | 0.17985 |
| 7.12 | 0.171536 | 0.176264 | 0.181037 | 0.191285 | 0.191143 | 0.191002 |
| 10 | 0.185906 | 0.191505 | 0.197159 | 0.209173 | 0.209038 | 0.208903 |
| 20 | 0.228769 | 0.236529 | 0.244408 | 0.261163 | 0.260962 | 0.260762 |
| 30 | 0.257672 | 0.266764 | 0.275949 | 0.295557 | 0.295327 | 0.295097 |
| 40 | 0.278551 | 0.288597 | 0.298703 | 0.320316 | 0.320053 | 0.31979 |
| 50 | 0.294436 | 0.305156 | 0.315986 | 0.339084 | 0.338828 | 0.338529 |
| 60 | 0.307127 | 0.318338 | 0.329704 | 0.353914 | 0.353621 | 0.353328 |
| 70 | 0.317403 | 0.329089 | 0.340853 | 0.366022 | 0.365691 | 0.365402 |
| 80 | 0.326 | 0.338028 | 0.350179 | 0.376076 | 0.375749 | 0.375422 |
| 90 | 0.333328 | 0.345649 | 0.358054 | 0.38458 | 0.384256 | 0.383932 |
| 100 | 0.339633 | 0.352198 | 0.364851 | 0.39187 | 0.391548 | 0.391227 |
| 200 | 0.374513 | 0.388365 | 0.402401 | 0.432339 | 0.432074 | 0.431389 |
| 300 | 0.389947 | 0.404348 | 0.419021 | 0.449934 | 0.449675 | 0.449416 |
| 400 | 0.398831 | 0.413575 | 0.428554 | 0.460407 | 0.459733 | 0.459478 |
| 500 | 0.404686 | 0.419754 | 0.43477 | 0.46711 | 0.466438 | 0.466185 |
| 600 | 0.408943 | 0.423874 | 0.43933 | 0.471718 | 0.471467 | 0.470797 |
| 700 | 0.412259 | 0.427169 | 0.442645 | 0.475489 | 0.47482 | 0.47457 |
| 800 | 0.414716 | 0.430053 | 0.445132 | 0.478421 | 0.477754 | 0.477505 |

Fig 4 illustrates how the electron cross-sectional area of the studied samples changes depending on the incident photon energies. A direct relationship was observed between the electron cross-sectional area and the mass-to-atomic-number ratio; the higher the mass-to-atomic-number ratio, the larger the cross-sectional area, and vice versa.

The data indicated that sample S4, composed of (60Pb40Bi), had the highest electron cross-sectional area, due to its highest mass-to-atomic-number ratio among the other samples. The results showed that sample S1, composed of (60Pb40Sn), had the lowest electron cross-sectional area, due to its lower mass-to-atomic-number ratio compared to the other samples.

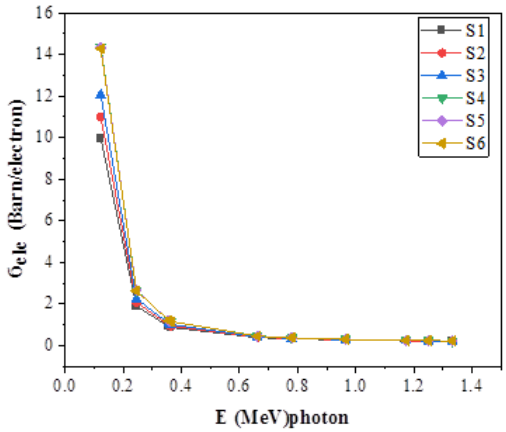


**Fig4: Electron cross-sectional area of the samples under study as a function of incident photon energies.**

**Table 5: Evaluate linear attenuation coefficient with incident photon energies.**

| E(MeV) | μ($cm^{-1}$) | | | | | |
|---|---|---|---|---|---|---|
| | S1 | S2 | S3 | S4 | S5 | S6 |
| 0.05953 | 55.98464 | 56.70321 | 57.29443 | 55.81964 | 56.39306 | 56.97065 |
| 0.08099 | 25.09824 | 25.55038 | 25.94524 | 25.56838 | 25.83187 | 26.09225 |
| 0.12178 | 23.66822 | 27.04977 | 30.62234 | 36.73445 | 37.13875 | 37.55034 |
| 0.24469 | 4.528384 | 5.122234 | 5.748404 | 6.800374 | 6.875453 | 6.950948 |
| 0.35601 | 2.1888 | 2.437519 | 2.698811 | 3.117284 | 3.15288 | 3.188195 |
| 0.364 | 2.107085 | 2.344313 | 2.592417 | 2.989764 | 3.023503 | 3.058064 |
| 0.66166 | 0.93739 | 1.011276 | 1.088162 | 1.191619 | 1.205705 | 1.2208 |
| 0.7789 | 0.796626 | 0.853435 | 0.912139 | 0.985872 | 0.998267 | 1.010716 |
| 0.96413 | 0.659753 | 0.701369 | 0.744227 | 0.792555 | 0.802788 | 0.812984 |
| 1.17323 | 0.565683 | 0.598236 | 0.631513 | 0.665249 | 0.674064 | 0.682743 |
| 1.25 | 0.541169 | 0.57149 | 0.602439 | 0.632994 | 0.641339 | 0.649659 |
| 1.3325 | 0.519281 | 0.547783 | 0.576842 | 0.604704 | 0.612746 | 0.620766 |
| 1.40801 | 0.502451 | 0.52975 | 0.557459 | 0.583486 | 0.591328 | 0.599041 |
| 2.75 | 0.39593 | 0.417701 | 0.4399 | 0.460681 | 0.466952 | 0.473101 |
| 7.12 | 0.407603 | 0.433505 | 0.460125 | 0.489293 | 0.495872 | 0.502436 |
| 10 | 0.441748 | 0.47099 | 0.501102 | 0.53505 | 0.542295 | 0.549525 |
| 20 | 0.543601 | 0.581722 | 0.62119 | 0.668035 | 0.676999 | 0.685942 |
| 30 | 0.61228 | 0.656084 | 0.701354 | 0.756014 | 0.76615 | 0.776261 |
| 40 | 0.661893 | 0.709778 | 0.759185 | 0.819345 | 0.830295 | 0.841216 |
| 50 | 0.699638 | 0.750504 | 0.803112 | 0.867353 | 0.879001 | 0.890511 |
| 60 | 0.729795 | 0.782924 | 0.83798 | 0.905288 | 0.917379 | 0.92944 |
| 70 | 0.754212 | 0.809366 | 0.866316 | 0.936257 | 0.948691 | 0.9612 |
| 80 | 0.774641 | 0.83135 | 0.890018 | 0.961975 | 0.974784 | 0.987557 |
| 90 | 0.792054 | 0.850092 | 0.910032 | 0.983729 | 0.996854 | 1.009944 |
| 100 | 0.807035 | 0.866201 | 0.927308 | 1.002375 | 1.015771 | 1.029133 |
| 200 | 0.889917 | 0.955151 | 1.022746 | 1.105891 | 1.120903 | 1.134781 |
| 300 | 0.926592 | 0.994459 | 1.064987 | 1.150898 | 1.166566 | 1.182202 |
| 400 | 0.947702 | 1.017152 | 1.089216 | 1.177688 | 1.192658 | 1.208669 |
| 500 | 0.961613 | 1.032349 | 1.105017 | 1.194834 | 1.210054 | 1.226314 |
| 600 | 0.97173 | 1.04248 | 1.116604 | 1.206622 | 1.2231 | 1.238444 |
| 700 | 0.97961 | 1.050585 | 1.125031 | 1.216266 | 1.231798 | 1.24837 |
| 800 | 0.985446 | 1.057676 | 1.131352 | 1.223767 | 1.239408 | 1.256089 |

Fig 5 shows how the linear attenuation coefficient of the tested samples changes depending on the incident photon energies. The results indicate that the linear attenuation coefficient increases with increasing sample density and decreases with decreasing sample density, indicating a direct relationship between the two.

This observation is supported by the results for individual samples. Sample S6, composed of (80Pb20Bi) and characterized by its highest density (11.028), exhibited the highest linear attenuation coefficient. In contrast, sample S1, composed of (60Pb40Sn) and characterized by its lowest density (9.728), recorded the lowest linear attenuation coefficient among all the samples studied.

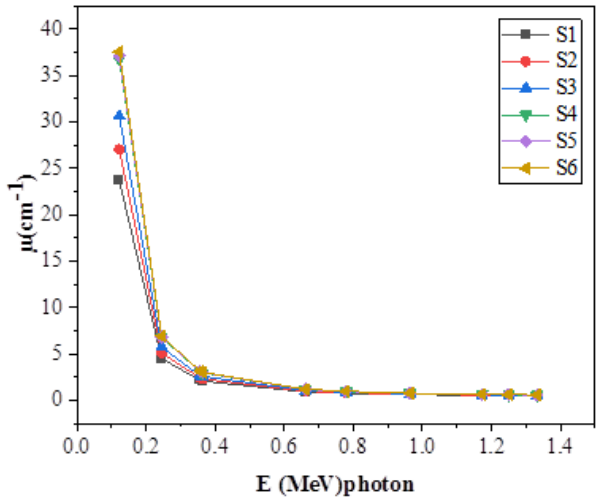


**Fig 5: Linear attenuation coefficient of the samples under study as a function of incident photon energies.**

**Table 6: Effective atomic number values of the samples under study .**

| $Z_{eff}$ | | | | | |
|---|---|---|---|---|---|
| S1 | S2 | S3 | S4 | S5 | S6 |
| 69.67538 | 72.8134 | 75.91305 | 82.39914 | 82.29925 | 82.19943 |

Fig 6 shows the behavior of the effective atomic number of the studied samples as a function of changing incident photon energies. It was observed that the effective atomic number is inversely proportional to the electron cross-sectional area and, conversely, directly proportional to the atomic cross-sectional area. This means that increasing the atomic cross-sectional area leads to a corresponding increase in the effective atomic number, and vice versa in the case of a decrease.

The results of the study confirm this relationship, as sample S4 (consisting of 60Pb40Bi) exhibited the highest effective atomic number and the highest atomic cross-sectional area (1183.335) compared to the other samples. Meanwhile, sample S1 (consisting of 60Pb40Sn) recorded the lowest effective atomic number, which corresponds to the lowest atomic cross-sectional area (694.0049) among the samples.

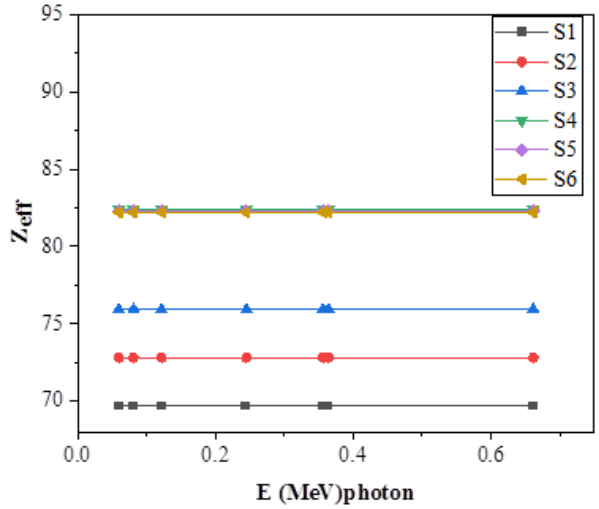


**Fig 6: Effective atomic number of the studied samples as a function of incident photon energies.**

**Table 7: Electron density values of the samples under study .**

| $N_{ele}*10^{23}$ | | | | | |
|---|---|---|---|---|---|
| S1 | S2 | S3 | S4 | S5 | S6 |
| 2.4426 | 2.4276 | 2.4176 | 2.367 | 2.3861 | 2.3853 |

Fig 7 shows the variation of electron density in the samples under study as a function of the incident photon energies. The results show a high degree of similarity in electron density values between the samples, indicating that this density does not change with the incident photon energy, as it depends primarily on the effective atomic number.

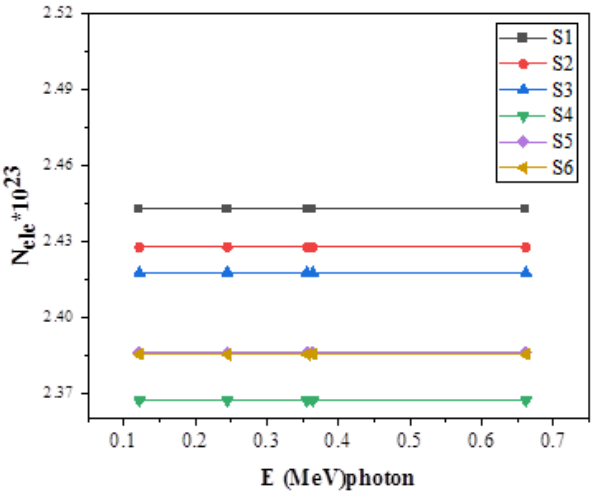


**Fig 7: Electron density of the samples under study as a function of the incident photon energies.**

**Table 8: Evaluate mean free path with incident photon energies.**

| E(MeV) | λ(cm) | | | | | |
|---|---|---|---|---|---|---|
| | S1 | S2 | S3 | S4 | S5 | S6 |
| 0.05953 | 0.017862 | 0.017636 | 0.017454 | 0.017915 | 0.017733 | 0.017553 |
| 0.08099 | 0.039843 | 0.039138 | 0.038543 | 0.039111 | 0.038712 | 0.038326 |
| 0.12178 | 0.042251 | 0.036969 | 0.032656 | 0.027222 | 0.026926 | 0.026631 |
| 0.24469 | 0.220829 | 0.195227 | 0.173961 | 0.147051 | 0.145445 | 0.143865 |
| 0.35601 | 0.456871 | 0.410253 | 0.370534 | 0.320792 | 0.31717 | 0.313657 |
| 0.364 | 0.474589 | 0.426564 | 0.38574 | 0.334475 | 0.330742 | 0.327004 |
| 0.66166 | 1.066792 | 0.988849 | 0.918981 | 0.839194 | 0.82939 | 0.819135 |
| 0.7789 | 1.255294 | 1.171735 | 1.096324 | 1.01433 | 1.001736 | 0.989397 |
| 0.96413 | 1.515719 | 1.425783 | 1.343676 | 1.261742 | 1.245658 | 1.230036 |
| 1.17323 | 1.767774 | 1.671582 | 1.583498 | 1.503196 | 1.483539 | 1.464679 |
| 1.25 | 1.847853 | 1.749813 | 1.659918 | 1.579794 | 1.559237 | 1.539268 |
| 1.3325 | 1.925741 | 1.82554 | 1.733577 | 1.653702 | 1.631998 | 1.610913 |
| 1.40801 | 1.990243 | 1.887683 | 1.793853 | 1.713837 | 1.691109 | 1.669335 |
| 2.75 | 2.525702 | 2.394056 | 2.273245 | 2.1707 | 2.141546 | 2.113713 |
| 7.12 | 2.453366 | 2.306776 | 2.173322 | 2.043767 | 2.01665 | 1.990305 |
| 10 | 2.263732 | 2.123186 | 1.9956 | 1.868985 | 1.844014 | 1.819753 |
| 20 | 1.839586 | 1.719034 | 1.609813 | 1.496927 | 1.477106 | 1.45785 |
| 30 | 1.633239 | 1.524196 | 1.425814 | 1.322727 | 1.305228 | 1.288227 |
| 40 | 1.510818 | 1.408892 | 1.317201 | 1.220487 | 1.204392 | 1.188756 |
| 50 | 1.429311 | 1.332437 | 1.245156 | 1.152933 | 1.137655 | 1.122951 |
| 60 | 1.370249 | 1.277264 | 1.193346 | 1.104621 | 1.090062 | 1.075917 |

| | | | | | | |
|---|---|---|---|---|---|---|
| 70 | 1.325887 | 1.235536 | 1.154313 | 1.068083 | 1.054084 | 1.040366 |
| 80 | 1.290921 | 1.202863 | 1.123573 | 1.039528 | 1.025869 | 1.012599 |
| 90 | 1.262541 | 1.176343 | 1.098862 | 1.01654 | 1.003156 | 0.990154 |
| 100 | 1.239104 | 1.154467 | 1.07839 | 0.997631 | 0.984474 | 0.971692 |
| 200 | 1.1237 | 1.046955 | 0.97776 | 0.904248 | 0.892138 | 0.881227 |
| 300 | 1.079224 | 1.005572 | 0.938978 | 0.868886 | 0.857217 | 0.845879 |
| 400 | 1.055184 | 0.983137 | 0.918092 | 0.849121 | 0.838463 | 0.827357 |
| 500 | 1.03992 | 0.968665 | 0.904964 | 0.836936 | 0.82641 | 0.815452 |
| 600 | 1.029093 | 0.959251 | 0.895573 | 0.82876 | 0.817595 | 0.807465 |
| 700 | 1.020815 | 0.951851 | 0.888864 | 0.822189 | 0.811822 | 0.801045 |
| 800 | 1.014769 | 0.945469 | 0.883899 | 0.817149 | 0.806837 | 0.796122 |

Fig 8 illustrates the dependence of the mean free path of the studied samples on the incident photon energies. The results indicate an inverse relationship between the mean free path and the linear attenuation coefficient; the mean free path value decreases with increasing attenuation coefficient. Sample S1, composed of (60Pb40Sn), was found to have the highest mean free path due to its lower linear attenuation coefficient compared to the other samples. In contrast, sample S6, composed of (80Pb20Bi), recorded the lowest mean free path due to its highest linear attenuation coefficient among the samples.

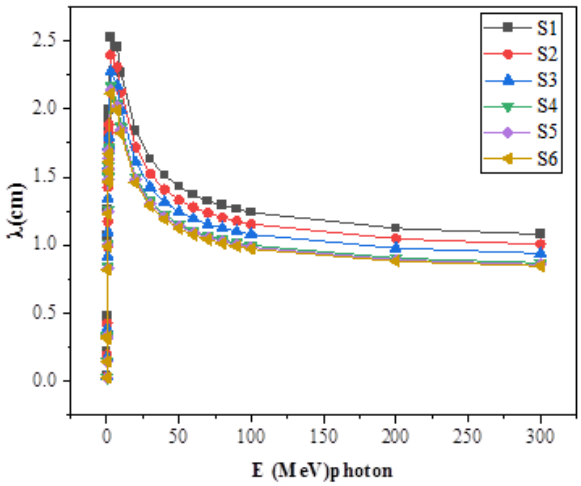


**Fig 8: Mean free path of the samples under study as a function of the incident photon energies.**

**Table 9: Evaluate half-value layer with incident photon energies.**

| E(MeV) | HVL(cm) | | | | | |
|---|---|---|---|---|---|---|
| | S1 | S2 | S3 | S4 | S5 | S6 |
| 0.05953 | 0.012381 | 0.012224 | 0.012098 | 0.012418 | 0.012291 | 0.012167 |
| 0.08099 | 0.027617 | 0.027129 | 0.026716 | 0.02711 | 0.026833 | 0.026565 |
| 0.12178 | 0.029286 | 0.025625 | 0.022635 | 0.018869 | 0.018664 | 0.018459 |
| 0.24469 | 0.153067 | 0.135321 | 0.120581 | 0.101928 | 0.100815 | 0.09972 |
| 0.35601 | 0.316679 | 0.284366 | 0.256834 | 0.222356 | 0.219846 | 0.21741 |
| 0.364 | 0.32896 | 0.295672 | 0.267375 | 0.23184 | 0.229253 | 0.226662 |
| 0.66166 | 0.739443 | 0.685418 | 0.636989 | 0.581685 | 0.574889 | 0.567781 |
| 0.7789 | 0.870103 | 0.812184 | 0.759914 | 0.70308 | 0.69435 | 0.685798 |
| 0.96413 | 1.050616 | 0.988277 | 0.931365 | 0.874573 | 0.863424 | 0.852596 |
| 1.17323 | 1.225327 | 1.158652 | 1.097597 | 1.041936 | 1.02831 | 1.015238 |
| 1.25 | 1.280834 | 1.212877 | 1.150567 | 1.095029 | 1.080781 | 1.066939 |

| | | | | | | |
|---|---|---|---|---|---|---|
| 1.3325 | 1.334822 | 1.265367 | 1.201624 | 1.146259 | 1.131214 | 1.116599 |
| 1.40801 | 1.379531 | 1.308442 | 1.243404 | 1.187941 | 1.172187 | 1.157094 |
| 2.75 | 1.750682 | 1.659433 | 1.575693 | 1.504615 | 1.484406 | 1.465114 |
| 7.12 | 1.700544 | 1.598935 | 1.506432 | 1.416631 | 1.397835 | 1.379574 |
| 10 | 1.569099 | 1.47168 | 1.383244 | 1.295481 | 1.278172 | 1.261356 |
| 20 | 1.275103 | 1.191543 | 1.115837 | 1.03759 | 1.023852 | 1.010504 |
| 30 | 1.132075 | 1.056492 | 0.988299 | 0.916845 | 0.904715 | 0.89293 |
| 40 | 1.047219 | 0.976569 | 0.913014 | 0.845977 | 0.834821 | 0.823982 |
| 50 | 0.990723 | 0.923575 | 0.863076 | 0.799152 | 0.788562 | 0.77837 |
| 60 | 0.949784 | 0.885332 | 0.827164 | 0.765665 | 0.755573 | 0.745769 |
| 70 | 0.919035 | 0.856408 | 0.800109 | 0.740339 | 0.730635 | 0.721126 |
| 80 | 0.894798 | 0.833761 | 0.778801 | 0.720546 | 0.711078 | 0.70188 |
| 90 | 0.875126 | 0.815379 | 0.761673 | 0.704612 | 0.695335 | 0.686322 |
| 100 | 0.858881 | 0.800215 | 0.747483 | 0.691505 | 0.682385 | 0.673525 |
| 200 | 0.778889 | 0.725694 | 0.677731 | 0.626777 | 0.618383 | 0.61082 |
| 300 | 0.748061 | 0.697009 | 0.65085 | 0.602266 | 0.594177 | 0.586319 |
| 400 | 0.731398 | 0.681458 | 0.636373 | 0.588566 | 0.581178 | 0.57348 |
| 500 | 0.720817 | 0.671427 | 0.627273 | 0.58012 | 0.572823 | 0.565228 |
| 600 | 0.713312 | 0.664902 | 0.620763 | 0.574453 | 0.566713 | 0.559692 |
| 700 | 0.707575 | 0.659773 | 0.616114 | 0.569898 | 0.562712 | 0.555242 |
| 800 | 0.703384 | 0.655349 | 0.612672 | 0.566404 | 0.559257 | 0.551829 |

Fig 9 represents the behavior of the half-thickness layer for the studied samples as a function of incident photon energies. The results show that the half-thickness layer has an inverse relationship with the linear attenuation coefficient; a higher linear attenuation coefficient leads to a lower value for the half-thickness layer, and vice versa. Sample S1, with a composition of (60Pb40Sn), was found to have the highest value for the half-thickness layer, attributed to its lower linear attenuation coefficient compared to the other samples. In contrast, sample S6, composed of (80Pb20Bi), recorded the lowest value for the half-thickness layer due to its highest linear attenuation coefficient among all studied samples.

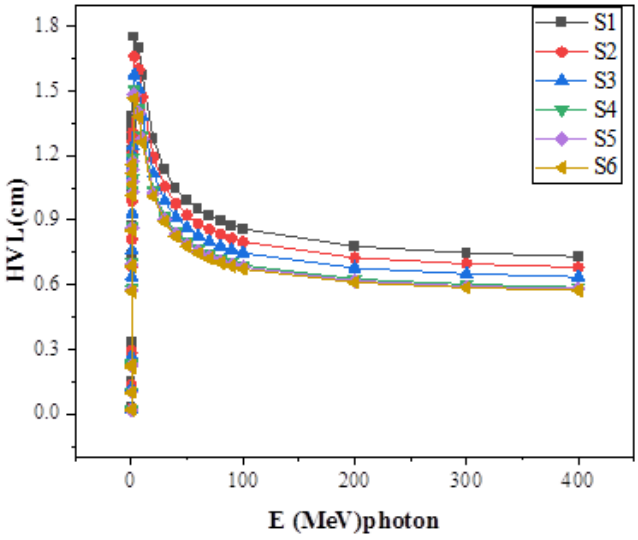


**Fig 9: Half-Value layer for the studied samples as a function of incident photon energies.**

**Table 10: Evaluate tenth layer thickness with incident photon energies.**

| E(MeV) | TVL(cm) |
|---|---|

| | S1 | S2 | S3 | S4 | S5 | S6 |
|---|---|---|---|---|---|---|
| 0.05953 | 0.041129 | 0.040608 | 0.040189 | 0.04125 | 0.040831 | 0.040417 |
| 0.08099 | 0.091743 | 0.090119 | 0.088748 | 0.090056 | 0.089137 | 0.088248 |
| 0.12178 | 0.097286 | 0.085124 | 0.075193 | 0.062682 | 0.062 | 0.06132 |
| 0.24469 | 0.508478 | 0.449528 | 0.400561 | 0.338597 | 0.334899 | 0.331262 |
| 0.35601 | 1.051985 | 0.944643 | 0.853185 | 0.738651 | 0.730312 | 0.722222 |
| 0.364 | 1.092782 | 0.9822 | 0.8882 | 0.770156 | 0.761562 | 0.752955 |
| 0.66166 | 2.456379 | 2.27691 | 2.116031 | 1.932316 | 1.909742 | 1.886129 |
| 0.7789 | 2.890422 | 2.698019 | 2.524379 | 2.335582 | 2.306582 | 2.278172 |
| 0.96413 | 3.490071 | 3.282986 | 3.093928 | 2.905267 | 2.868234 | 2.832263 |
| 1.17323 | 4.07045 | 3.84896 | 3.646139 | 3.461237 | 3.415974 | 3.372548 |
| 1.25 | 4.254838 | 4.029093 | 3.822102 | 3.637609 | 3.590276 | 3.544295 |
| 1.3325 | 4.434182 | 4.203461 | 3.991709 | 3.80779 | 3.757814 | 3.709263 |
| 1.40801 | 4.582704 | 4.34655 | 4.130499 | 3.946255 | 3.893921 | 3.843786 |
| 2.75 | 5.815642 | 5.512518 | 5.234339 | 4.998222 | 4.931091 | 4.867003 |
| 7.12 | 5.649085 | 5.311547 | 5.004258 | 4.705947 | 4.643508 | 4.582845 |
| 10 | 5.212434 | 4.888817 | 4.595039 | 4.303496 | 4.245998 | 4.190135 |
| 20 | 4.235803 | 3.958222 | 3.706732 | 3.446801 | 3.401162 | 3.356824 |
| 30 | 3.760671 | 3.509591 | 3.283058 | 3.045692 | 3.005398 | 2.966251 |
| 40 | 3.478787 | 3.244092 | 3.03968 | 2.810274 | 2.773214 | 2.737211 |
| 50 | 3.29111 | 3.06805 | 2.867078 | 2.654726 | 2.619547 | 2.58569 |
| 60 | 3.155114 | 2.941008 | 2.747781 | 2.543484 | 2.509959 | 2.47739 |
| 70 | 3.052969 | 2.844926 | 2.657904 | 2.459352 | 2.427119 | 2.39553 |
| 80 | 2.972456 | 2.769694 | 2.587123 | 2.393601 | 2.36215 | 2.331596 |
| 90 | 2.907107 | 2.70863 | 2.530223 | 2.340671 | 2.309853 | 2.279913 |
| 100 | 2.853142 | 2.658259 | 2.483085 | 2.29713 | 2.266835 | 2.237403 |
| 200 | 2.587414 | 2.410703 | 2.251375 | 2.082108 | 2.054223 | 2.0291 |
| 300 | 2.485004 | 2.315415 | 2.162077 | 2.000685 | 1.973815 | 1.947709 |
| 400 | 2.429651 | 2.263756 | 2.113985 | 1.955173 | 1.930632 | 1.905059 |
| 500 | 2.394503 | 2.230433 | 2.083756 | 1.927117 | 1.902879 | 1.877648 |
| 600 | 2.369573 | 2.208757 | 2.062132 | 1.908291 | 1.882581 | 1.859256 |
| 700 | 2.350513 | 2.191718 | 2.046685 | 1.893159 | 1.869288 | 1.844474 |
| 800 | 2.336591 | 2.177022 | 2.035251 | 1.881555 | 1.85781 | 1.833138 |

Figure 10 shows the behavior of the tenth layer thickness (Tenth Value Layer, or TVL) for the samples under study as a function of incident photon energies. The results revealed a clear inverse relationship between the tenth layer thickness and the linear attenuation coefficient; the higher the linear attenuation coefficient, the lower the tenth layer thickness, and vice versa. This is because the linear attenuation coefficient represents the ability of a material to reduce radiation intensity through absorption or scattering. Therefore, materials with high attenuation coefficients require a smaller thickness to achieve a significant reduction in photon intensity . Sample S1, composed of (60Pb40Sn), showed the highest value for the tenth layer thickness due to its lower linear attenuation coefficient compared to the other samples. Sample S6, composed of (80Pb20Bi), recorded the lowest value for the tenth layer thickness due to its high linear attenuation coefficient. These results are of great practical importance in the design of radiation shields, as the tenth-layer thickness is used as a benchmark for determining the thickness of shielding materials required to reduce radiation intensity to one-tenth of its original value. Therefore, choosing materials with high linear attenuation coefficients allows for reducing the required shield thickness, contributing to improved efficiency and reducing cost and space.

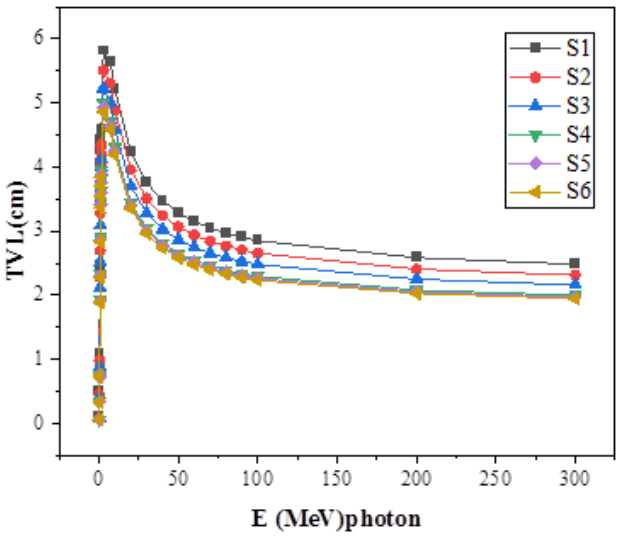


**Fig 10: Tenth layer thickness for the studied samples as a function of incident photon energies.**

## 4. Conclusion

By evaluating a set of gamma ray protection parameters, including mass attenuation coefficient, molecular and electron cross-sectional area, linear attenuation coefficient, effective atomic number, electron density, mean free path, and layer thickness for Pb-Bi and Pb-Sn alloys with varying component ratios, the following conclusions were reached:

- Most of the gamma-ray shielding properties of the studied samples are closely related to the mass attenuation coefficient, which in turn depends on the incident photon energy, showing high values at low energies and then decreasing significantly with increasing energy.
- At high energies around E>100MeV, most shielding parameters exhibit attenuation stability.
- The elements that make up the studied alloys exhibit distinct absorption edges as follows:

1. Lead (Pb): The M-type absorption edge lies between 0.002484 and 0.003851 MeV, the L-type edge lies between 0.01304 and 0.01586 MeV, and the K-type absorption edge lies at 0.088 MeV.
2. Bismuth (Bi): The M-type absorption edge lies between 0.00258 and 0.003999 MeV, the L-type edge lies between 0.01304 and 0.01639 MeV, and the K-type edge lies at 0.09053 MeV.
3. Tin (Sn): The L-type absorption edge lies between 0.003929 and 0.004465 MeV, and the K-type edge lies at 0.2920 MeV.

- Sample S1, with composition (60Pb40Sn), recorded the highest values for mean free path (0.042251), half layer thickness (0.029286), and tenth layer thickness (0.097286), while it recorded the lowest value for linear attenuation coefficient (23.66822).
- Sample S6, with composition (80Pb20Bi ), exhibited excellent attenuation properties, recording the lowest mean free path (0.026631), half layer thickness (0.018459 ), and tenth layer thickness (0.06132). Concurrently, this sample had the highest mass attenuation coefficient (3.405). Together, these results indicate that sample S6 is the ideal alloy choice for gamma-ray shielding applications, due to its superior radiation attenuation capability.

**Reference**

1. Abdel-Rahman, W., & Podgorsak, E. B., Energy transfer and energy absorption in photon interactions with matter revisited: A step-by-step illustrated approach. Radiation Physics and Chemistry. 79(5),552-566. (2010).
2. Brown, Saxby, Dale L. Bailey, Kathy Willowson, and Clive Baldock. "Investigation of the relationship between linear attenuation coefficients and CT Hounsfield units using radionuclides for SPECT." Applied Radiation and Isotopes 66, no. 9 (2008): 1206-1212.
3. Taqi, Ali H., Abdulahdi M. Ghalib, and Hilala N. Mohammed. "Shielding properties of Cu-Sn-Pb alloy by Geant4, XCOM and experimental data." *Materials Today Communications* 26 (2021): 101996.
4. Sharma, R., Sharma, J.K., Singh, T., 2016. Effective atomic numbers for some alloys at 662 keV using gamma rays backscattering technique. Phys. Sci. Int. J.11 (1),1e6.
5. Kaur, Preet, Devinder Singh, and Tejbir Singh. "Heavy metal oxide glasses as gamma rays shielding material." Nuclear Engineering and design 307 (2016): 364-376.
6. Han, I., Demir, L., 2009a. Studies on effective atomic number, electron density from mass attenuation coefficients in TixCo1-x and CoxCu1-x alloys. Nucl. Instrum. Methods. B 267, 21e22.
7. Singh, Tejbir, Amandeep Kaur, Jeewan Sharma, and Parjit S. Singh. "Gamma rays' shielding parameters for some Pb-Cu binary alloys." Engineering science and technology, an international journal 21, no. 5 (2018): 1078-1085.
8. Tam, D. K. Y., S. Ruan, Ping Gao, and Tongxi Yu. "High-performance ballistic protection using polymer Nano composites." In Advances in military textiles and personal equipment, pp. 213-237. Woodhead Publishing, 2012.
9. Elias, Hans-Georg, and Hans-Georg Elias. "Determination of molecular weight and molecular-weight distribution." Macromolecules: Volume 1· Structure and Properties (1977): 297-369.
10. Akça, B., & Erzeneoğlu, S. Z., The mass attenuation coefficients, electronic, atomic, and molecular cross sections, effective atomic numbers, and electron densities for compounds of some biomedically important elements at 59.5 keV. Science and Technology of Nuclear Installations, 1-8. (2014).
11. Manohara, S. R., Hanagodimath, S. M., & Gerward, L., Energy dependence of effective atomic numbers for photon energy absorption and photon interaction: studies of some biological molecules in the energy range 1 keV-20 MeV: Effective atomic numbers of some biological molecules. Medical Physics, 35(1),388-402. (2008).
12. Kaur, Sarpreet, Amandeep Kaur, Parjit S. Singh, and Tejbir Singh. "Scope of Pb-Sn binary alloys as gamma rays shielding material." *Progress in Nuclear Energy* 93 (2016): 277-286.
13. Ibrahim K. A., Allah, S. M. A. (2025). The influence of chemical composition on the shielding coefficients for different materials to gamma rays and fast neutrons. Central Asian journal of medical and natural sciences 6(2), 762-774. Kirkuk university
14. Nuri, Z.M., Aziz, A.A., Mahmoud, S., & Allah, A. (2024). Investigation of the Protective Armours for Gamma Rays and Fast Neutrons Parameters. Nanotechnology Perceptions. Kirkuk university.
15. Masterson, R. E. (2017). *Nuclear engineering fundamentals: a practical perspective*. CRC Press.